IMECE2007-42619

EFFECTS OF CREEP FLOW AND VISCOUS DISSIPATION IN THE SLIP REGIME FOR ISOFLUX RECTANGULAR MICROCHANNELS

Jennifer van Rij, Tim Ameel, Todd Harman
Department of Mechanical Engineering
University of Utah, Salt Lake City, Utah

ABSTRACT

The effects of rarefaction on convective heat transfer and pressure drop characteristics are numerically evaluated for uniform wall heat flux rectangular microchannels. Results are obtained by numerically solving the momentum and energy equations with both first- and second-order slip velocity and temperature jump boundary conditions. The resulting velocity and temperature fields are then evaluated to obtain the microchannel Poiseuille and Nusselt numbers. In addition to the effects of rarefaction, the effects of aspect ratio, thermal creep flow, and viscous dissipation are investigated for locally fully developed Poiseuille and Nusselt numbers. The constant wall heat flux results obtained in this study are compared to constant wall temperature results obtained previously, using the same numerical algorithm, at various aspect ratios including the limiting case of parallel plate microchannels. In addition to supplying previously unreported data on slip flow convective heat transfer and pressure drop characteristics, these results verify the numerical algorithm for more complex future slip flow analyses.

NOMENCLATURE

AR	aspect ratio, b/h
b	one-half the channel width
Br	Brinkman number,
	$Br_{H2} = \mu u_m^2 / q_w^{"} D_h$, $Br_T = \mu u_m^2 / k(T_i - T_w)$
c_p	specific heat at constant pressure
D_h	hydraulic diameter, $4hb/(h+b)$
f	friction factor, $8\tau_{w,avg} / \rho u_m^2$
h	one-half the channel height
k	thermal conductivity
L	channel length
Kn	Knudsen number, λ/D_h
Ma	Mach number, $(Pe \cdot Kn/Pr)\sqrt{2/\pi\gamma}$
Nu	Nusselt number, $q_{w,avg}^{"} D_h / k(T_w - T_m)$
Pe	Peclet number, $Pr \cdot Re$
Po	Poiseuille number, $f \cdot Re$
Pr	Prandtl number, $c_p \mu / k$
$q_w^{"}$	heat flux normal to the wall
R	gas constant
Re	Reynolds number, $\rho u_m D_h / \mu$
T	fluid temperature
T_i	inlet temperature
T_m	mixed mean temperature
T_w	wall temperature
u	streamwise velocity
u_c	creep velocity, $(3/4)(\mu/\rho T)(\partial T/\partial x)\big|_{y=0}$
u_m	mean velocity
v	wall normal velocity
x, y, z	Cartesian coordinates

Greek Symbols

β	gas/wall interaction parameter, β_t / β_v
β_t	first-order temperature jump coefficient, $(2 - \sigma_t/\sigma_t)(2\gamma/1+\gamma)(1/Pr)$
β_v	first-order velocity slip coefficient, $(2-\sigma_v)/\sigma_v$
$\beta_v Kn$	rarefaction parameter
γ	ratio of specific heat capacities
λ	molecular mean free path, $\mu/(\rho\sqrt{2RT/\pi})$
μ	dynamic viscosity
ρ	density
σ_t	thermal accommodation coefficient
σ_v	momentum accommodation coefficient
τ_w	wall shear stress

Subscripts

$H2$	constant wall heat flux thermal boundary condition
o	nominal continuum value
T	constant wall temperature thermal boundary condition

INTRODUCTION

Many technological advances in computation speed, power supply requirements, diagnostics, and control issues are contingent on the reduction of thermal fluid systems to the microscale. However, as thermal fluid system sizes are reduced, effects that are negligible at a macroscale may become significant, and thus change the predicted behavior of these systems at a microscale. For gaseous flows, some of these effects include compressibility, rarefaction, and viscous dissipation. Fundamental to the design of many thermal fluid systems is the accurate evaluation of pressure losses and convective heat transfer rates. As such, the assessment of these characteristics in microchannels has been an active area of research.

The most common means of analytically or numerically modeling a rarified flow within the slip regime is through the use of slip velocity and temperature jump boundary conditions applied to the conventional continuum momentum and energy equations. The original slip velocity boundary condition, given in Eq. (1), and temperature jump boundary condition, given in Eq. (2), were derived by Maxwell [1] and Smoluchowski [2], respectively.

$$u\big|_{y=0} - u_w = \left[\left(\frac{2-\sigma_v}{\sigma_v} \right) \lambda \left(\frac{\partial u}{\partial y} + \frac{\partial v}{\partial x} \right) + \frac{3}{4} \frac{\mu}{\rho T} \frac{\partial T}{\partial x} \right]_{y=0} \quad (1)$$

$$T\big|_{y=0} - T_w = \left[\left(\frac{2-\sigma_t}{\sigma_t} \right) \left(\frac{2\gamma}{1+\gamma} \right) \frac{\lambda}{Pr} \frac{\partial T}{\partial y} \right]_{y=0} \quad (2)$$

The first term in Eq. (1) is the velocity slip due to the shear stress at the wall, and the second term is the thermal creep velocity, u_c, due to a temperature gradient tangential to the wall. Equations (1) and (2), as well as subsequent equations, are presented in a format assuming a Cartesian coordinate system, a wall normal direction (y), and a streamwise direction (x). To reduce the number of variables involved, the nondimensional parameters β_v, β_t, $\beta_v Kn$, and β, as defined in the nomenclature, are used hereafter, rather than the coefficients of Eqs. (1) and (2). $\beta_v Kn$ is representative of the level of rarefaction, where $\beta_v Kn = 0$, corresponds to continuum conditions, and $\beta_v Kn \approx 0.10$, corresponds to the approximate upper limit of the slip regime. β is representative of the gas/wall interactions, where $\beta = 0$ corresponds to the artificial condition of zero temperature jump with nonzero slip velocity, $\beta \approx 1.667$ corresponds to typical values for air ($\gamma = 1.4$, $Pr = 0.7$) when $\sigma_v = \sigma_t = 1$, and β values as high as 100 are possible.

The boundary conditions given in Eqs. (1) and (2) are first-order approximations, in Kn, and only applicable in the slip flow regime. In an attempt to improve the accuracy of the first-order slip model given in Eqs. (1) and (2), and extend the continuum equations' range of applicability into the lower transition regime numerous modifications and second-order slip models have been proposed. The boundary conditions derived by Deissler [3], given in Eqs. (3) and (4), and the boundary conditions suggested by Karniadakis and Beskok [4], given in Eqs. (5) and (6), are two of the more common second-order slip boundary condition models.

$$u\big|_{y=0} - u_w = \left[\beta_v \lambda \frac{\partial u}{\partial y} - \frac{9}{16} \lambda^2 \left(2\frac{\partial^2 u}{\partial y^2} + \frac{\partial^2 u}{\partial x^2} + \frac{\partial^2 u}{\partial z^2} \right) \right]_{y=0} \quad (3)$$

$$T\big|_{y=0} - T_w =$$
$$\left[\beta_t \lambda \frac{\partial T}{\partial y} - \frac{9\lambda^2}{256} \left(\frac{177\gamma-145}{\gamma+1} \right) \left(2\frac{\partial^2 T}{\partial y^2} + \frac{\partial^2 T}{\partial x^2} + \frac{\partial^2 T}{\partial z^2} \right) \right]_{y=0} \quad (4)$$

$$u\big|_{y=0} - u_w = \beta_v \left[\lambda \frac{\partial u}{\partial y} + \frac{\lambda^2}{2} \frac{\partial^2 u}{\partial y^2} \right]_{y=0} \quad (5)$$

$$T\big|_{y=0} - T_w = \beta_t \left[\lambda \frac{\partial T}{\partial y} + \frac{\lambda^2}{2} \frac{\partial^2 T}{\partial y^2} \right]_{y=0} \quad (6)$$

Previous studies have shown second-order boundary conditions to be useful in some cases with respect to evaluating microchannel velocity profiles [4], mass flow rates, and/or pressure distributions [5,6]. However, before any conclusions regarding the usefulness or accuracy of any particular second-order slip boundary condition model is made, its ability to accurately predict convective heat transfer must also be assessed. Currently, experimental data on convective heat transfer rates within the slip flow regime do not exist. The majority of previous microchannel studies have analytically or numerically evaluated the effects of rarefaction using first-order velocity slip and temperature jump boundary conditions. Although, several recent studies have used second-order slip boundary conditions to evaluated pressure loss and convective heat transfer rates [4,7-12], the particular case of a rectangular microchannel geometry with constant axial and peripheral heat flux (*H2* thermal boundary condition) has not yet been reported.

While creep flow is typically negligible for a fully developed, constant wall temperature flow, creep effects may become significant for constant wall heat flux flows within the slip regime. For a parallel plate geometry with constant wall heat flux boundary conditions, the effect of creep flow has been shown to significantly alter the pressure losses and convective heat transfer rates from that predicted when creep flow is neglected [9,10]. However, the effect of creep flow on fully developed, constant wall heat flux, rectangular microchannel pressure losses and convective heat transfer rates has been neglected in previous studies.

Because the function of many microfluidic systems is cooling, viscous dissipation becomes a limiting factor that must be accurately represented. The Brinkman number is typically used to characterize the magnitude of viscous dissipation and flow work for a gaseous flow. In macroscale systems, viscous dissipation effects are only significant for high velocity or highly viscous flows. However, in microscale flows viscous dissipation effects may also become significant due to small temperature gradients and very large ratios of channel length to hydraulic diameter, which result in large velocity and pressure gradients. Recently, several studies have focused specifically on viscous dissipation effects for slip flow convective heat transfer [11-19]. However, the effect of viscous dissipation on rectangular microchannels with *H2* thermal boundary conditions has not yet been reported.

Copyright © 2007 by ASME

The objectives of this study are to numerically evaluate the effects of rarefaction on convective heat transfer and pressure drop characteristics for rectangular microchannels with uniform wall heat flux (H2 thermal boundary conditions). First- and second-order slip velocity and temperature jump boundary conditions are used with the continuum momentum and energy equations to numerically obtain the local thermally and hydrodynamically fully developed microchannel velocities and temperatures. The effects of aspect ratio, rarefaction, gas/wall interactions, creep flow, and viscous dissipation with flow work on convective heat transfer rates and friction loads are then evaluated through the Nusselt number, Nu, and Poiseuille number, Po, respectively. Additionally, the constant wall heat flux results are compared to previously obtained constant wall temperature results [12].

COMPUTATIONAL MODEL

The computational fluid dynamics (CFD) algorithm used for this study has been described, and verified for previous microchannel investigations [10-12]. The algorithm is based on ICE (Implicit, Continuous-fluid Eulerian), which is a finite volume, multi-material CFD method. The ICE implementation used in this study is well developed and documented [20-22]. The code is three-dimensional, fully compressible, unsteady, and capable of modeling variable fluid properties, fluid-structure interactions, and chemical reactions. To accurately model microchannel flows, the algorithm has been modified to optionally model any of the first- or second-order slip boundary conditions models presented in Eqs. (1) – (6), creep flow, and viscous dissipation. The implementation of these modifications is consistent with the original code in being numerically second-order accurate both spatially and temporally.
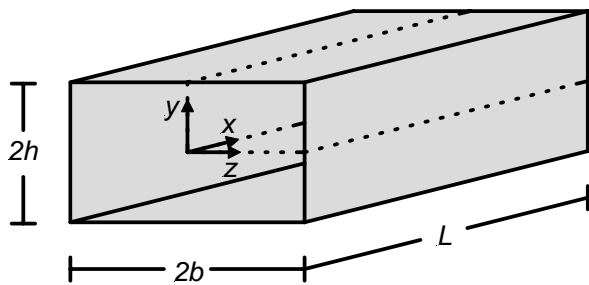

Figure 1. Channel geometry.

Numerical results are obtained for the three-dimensional, continuum, momentum and energy equations with both first- and second-order slip velocity and temperature jump boundary conditions for the flow configuration illustrated in Fig. 1. The flow is modeled assuming laminar flow of a Newtonian, ideal gas, with constant properties (c_p, k, μ) of air. To decrease the computational time required to reach a solution, only one quarter of the symmetric microchannel is modeled. The resulting velocity field is then evaluated to obtain the Poiseuille number, Po, which is an indication of the pressure drop characteristics and the temperature field is evaluated to obtain the Nusselt number, Nu, which represents the convective heat transfer characteristics.

Solution Criteria

For the numerical solutions to be comparable to previous first-order analytic solutions [23,24], the flow must be nearly incompressible. To achieve this criterion, a Mach number of approximately 0.05 or less is maintained. For the low Pe values used in this study, a channel length of $12h$ is found to be sufficient for Po and Nu values to become locally fully developed while avoiding significant compressibility effects due to a longer channel. For all cases, a uniform inlet velocity and temperature are specified while the outlet temperature and velocity profiles are allowed to evolve to their locally fully developed profiles. The inlet velocity, inlet temperature, outlet pressure, and wall temperature or wall heat flux are specified to obtain the desired flow Pe, u_c/u_m, Br_{H2} or Br_T, and Kn.

Because the algorithm is unsteady, all of the flow properties must evolve from a set of initial values to steady state conditions subject to the boundary conditions. The initial velocity field is zero and the initial temperature field is equal to the inlet temperature. The convergence criteria for each time step is a mass flux residual less than 10^{-10} for each control volume. The criterion used to establish that the flow is steady state is, $\left|\left(u^{n+1} - u^n\right)/u^{n+1}\right| \leq 10^{-10}$ and $\left|\left(T^{n+1} - T^n\right)/T^{n+1}\right| \leq 10^{-10}$, for each control volume, where n is the number of the time step. The magnitude and number of time steps required to reach steady state are dependent on the grid resolution, $\beta_v Kn$, and Pe.

Grid Convergence

To assure that each numerical result is sufficiently accurate and converges to a grid independent solution, grid resolution studies have been completed for each numerical Po and Nu. Table 1 presents the grid resolution studies for Nu_{H2} with $\beta_v Kn = 0$, and $AR = 1$, 2, and 5. For each aspect ratio the relative change in Nu_{H2} is less than 0.5% between the two highest grid resolutions. These data indicate that the numerical algorithm converges with approximately second-order numerical accuracy, and that the highest grid resolution tested for each AR, is sufficiently accurate. Based on these data, all of the following results are obtained using the finest grid resolution given in Table 1.

Table 1. Grid resolution effects on rectangular channel, continuum flow Nu_{H2} with comparison to analytic solutions.

AR	grid resolution	Nu_{H2} present	Nu_{H2} [23]	Nu_{H2} [24]	Nu_{H2} [25]	Nu_{H2} [26]
1	$60\times10\times10$	3.175				
	$120\times20\times20$	3.108	3.10	3.135	3.09	3.091
	$240\times40\times40$	3.092				
2	$60\times10\times20$	3.070				
	$120\times20\times40$	3.031	3.03	3.065	3.02	3.022
	$240\times40\times80$	3.022				
5	$60\times10\times50$	2.964				
	$120\times20\times100$	2.936	2.90	2.961	2.93	2.922
	$240\times40\times200$	2.929				

3   Copyright © 2007 by ASME

Code Verification

The algorithm's ability to model first- and second-order velocity slip and temperature jump boundary conditions as well as creep flow and viscous dissipation has been verified previously for two-dimensional flows with either constant wall heat flux or constant wall temperature boundary conditions [10,11]. For rectangular microchannel flows with a constant wall temperature boundary condition, the algorithm's ability to model first- and second-order velocity slip and temperature jump with viscous dissipation and axial conduction was verified in [12]. To verify that the algorithm also accurately models rectangular microchannel flows with constant wall heat flux boundary conditions, the numerically computed first-order slip Nu_{H2}, without viscous dissipation or creep flow effects, are compared to the analytically computed values given by [23] and [24] in Figure 2.
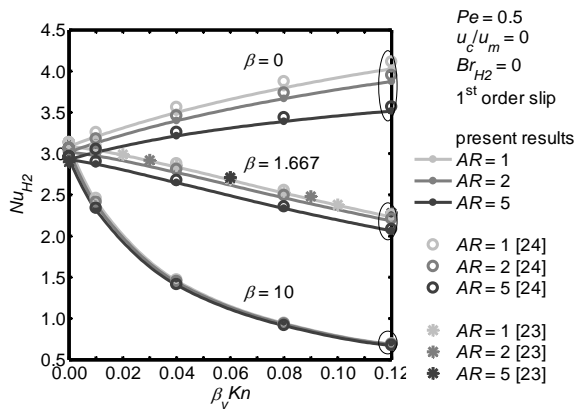
Figure 2. Comparison of numerically and analytically computed Nu_{H2} for rectangular channel first-order slip flow.

Although, this comparison demonstrates that the numerically computed Nu_{H2} values closely agree with the analytically computed values of [24], for all values of $\beta_v Kn$, β, and AR investigated, the numerical values are an average of 1.26% lower. However, referring to the data presented in Table 1 for continuum flow, the values given by [24] are an average of 1.39% higher than all other references [23,25,26], while the average difference between the numerically computed values, at the highest grid resolution, and all other references [23,25,26] is negligible. Based on this observation, it is assumed that while the differences between the analytical values of [24] and the present numerically computed values are slight, the numerically computed values are more accurate. The analytically computed values of [23] for $\beta = 1.667$ and $AR = 1$ are all within 0.5% of the present numerical data. However, for $AR = 2$ and 5 there is nearly a 10% difference between some of the analytic and numeric data. This discrepancy is attributed to the fact the Nu_{H2} values of [23] were derived with Kn defined as $\lambda/2b$, rather than the current definition, $Kn = \lambda/D_h$. Although this has been accounted for in presenting and comparing the data of Fig. 4, it appears that some accuracy in the analytic solution is lost under the current definition. Because the numerical data follow the expected AR trends, the current numerical solutions are again assumed to be more accurate, at least for the current definition of Kn.

RESULTS AND DISCUSSION

An evaluation and summary of the effects of first- and second-order slip boundary condition models, creep flow, and viscous dissipation on rectangular microchannel pressure drop and convective heat transfer characteristics are presented in Figs. 3 - 7. All Po and Nu are normalized by nominal continuum values without creep flow or viscous dissipation effects, Po_o and Nu_o, respectively. All numerically computed values are specified by symbols, with the connecting lines representing the data trend. All other relevant flow parameters are indicated in the Figures.

Rarefaction Effects

Fully developed Po/Po_o, for the different slip flow boundary condition models, are presented in Fig. 3 for $AR = 1$, 2, 5, and ∞. The boundary conditions are first-order slip [1,2], Eqs. (1) and (2), second-order Deissler slip [3], Eqs. (3) and (4), and second-order Karniadakis and Beskok slip [4], Eqs. (5) and (6). For these data $Pe = 0.5$, $Br_{H2} = 0$, and $u_c/u_m = 0$.

The data in Fig. 3 indicate that Po/Po_o decreases with $\beta_v Kn$ for all AR, and that the effect of AR on Po is significant in both the continuum and slip flow regimes. Within the continuum flow regime, Po_o decreases from 96, for $AR = \infty$, to 56.9, for $AR = 1$, due to the reduced average wall shear stress caused by the proximity of the corners. Within the slip flow regime, increasing rarefaction, $\beta_v Kn$, increases the slip velocity at the walls, which results in a flatter velocity profile with reduced wall velocity gradients and consequently reduces Po/Po_o for all AR. Although Po/Po_o decreases with $\beta_v Kn$ for all AR, the slip velocity is a function of both $\beta_v Kn$ and the average wall velocity gradients, which are larger for higher AR flow, and as a result Po/Po_o decreases more significant for higher AR flows.

The data in Fig. 3 also illustrate that second-order slip terms become more significant as $\beta_v Kn$ increases. However, the two second-order models have opposite effects when compared to the first-order boundary condition data. This result is expected, due to the opposite signs of the second-order coefficients, given in Eqs. (3) and (5). As compared to the first-order boundary condition data, the second-order Deissler boundary conditions result in an increase in the slip velocity and consequently reduce Po/Po_o with $\beta_v Kn$, while the second-order Karniadakis and Beskok boundary conditions result in a decrease in the slip velocity and consequently increase Po/Po_o with $\beta_v Kn$. Second-order effects are more significant for larger AR due, again, to the larger average wall velocity gradients.
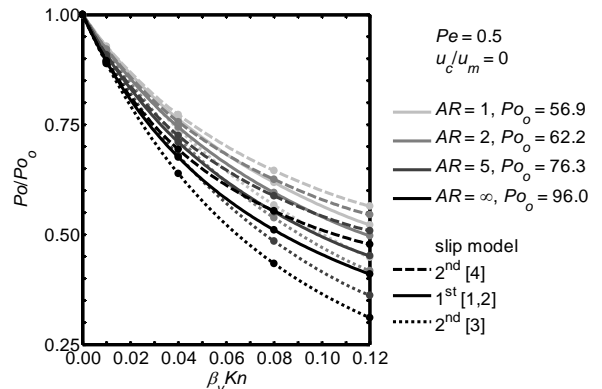
Figure 3. Effect of first- and second-order slip boundary conditions on fully developed Po/Po_o.

4   Copyright © 2007 by ASME

a)

b)

c)

d)
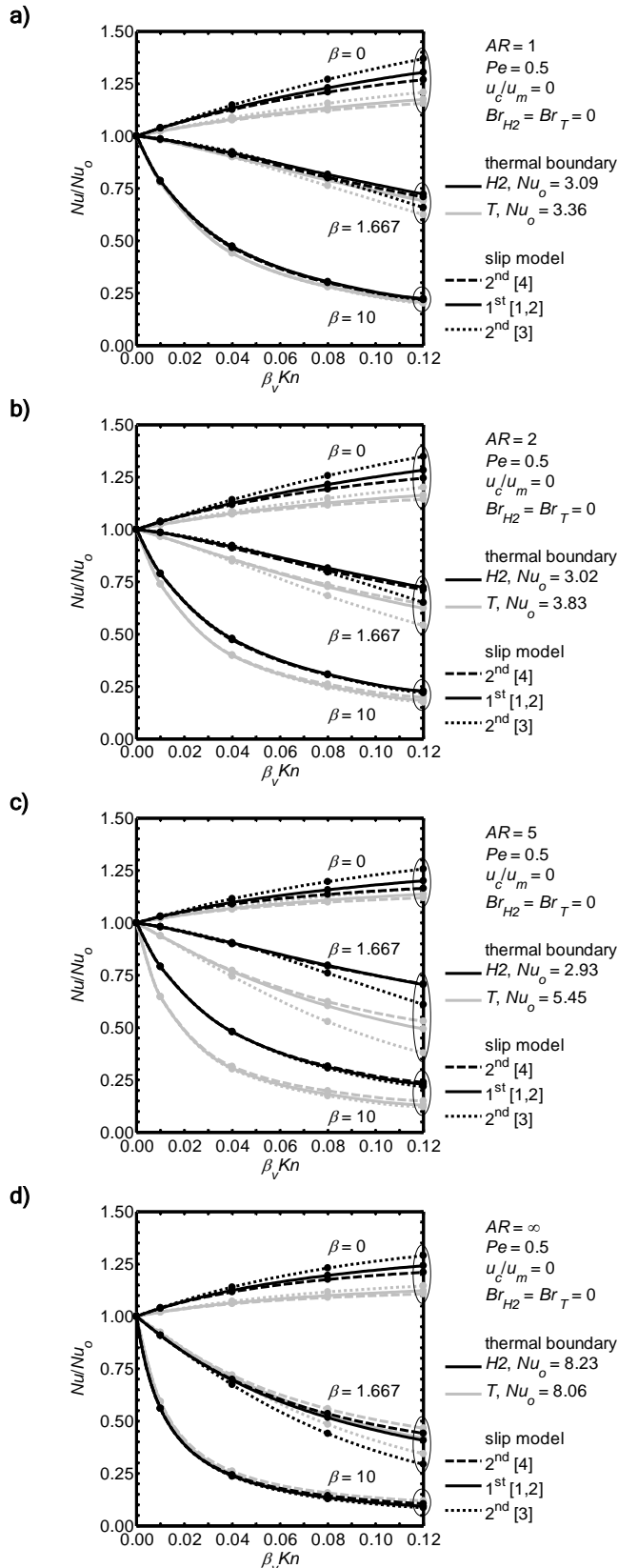
Figure 4. Effect of first- and second-order slip boundary conditions on fully developed Nu_{H2}/Nu_o and Nu_T/Nu_o. a) $AR = 1$, b) $AR = 2$, c) $AR = 5$, d) $AR = \infty$

Fully developed Nu_{H2} and Nu_T are presented in Fig. 4 for the same slip flow boundary condition models, Pe, Br_{H2}, Br_T, u_c/u_m, and AR values as in Fig. 3. The data in Fig. 4 indicate that both Nu_T and Nu_{H2} may increase or decrease with $\beta_v Kn$, depending on β, for all AR investigated, and that the effect of AR on Nu_T is more significant in both the continuum and the slip flow regimes than it is for Nu_{H2}. Within the continuum flow regime Nu_T, increases significantly from 3.36, at $AR = 1$, to 8.06, at $AR = \infty$ ($Pe = 0.5$). This variation is due to the reduced average wall heat flux caused by the proximity of the corners at lower AR. Nu_{H2} however, is nearly constant with respect to AR, i.e., it decreases approximately 6% from 3.09, at $AR = 1$, to 2.91, at $AR = 10$, and does not approach the $AR = \infty$ value of $Nu_{H2} = 8.235$ [25]. This behavior is due to the $H2$ boundary condition, for which the heat flux is constant both axially and peripherally, and as such the heat flux on the two side walls will always have an effect, even at large AR, and the average wall heat flux remains unchanged, even for small AR.

The data trends in Fig. 4 for the slip flow regime are related to the fact that as rarefaction, $\beta_v Kn$, increases, both the slip velocity and the temperature jump at the wall increase, for $\beta \neq 0$. An increase in the slip velocity enhances the energy exchange near the wall, which tends to increase both Nu_T and Nu_{H2}, as displayed when $\beta = 0$. However, for $\beta \neq 0$, increasing $\beta_v Kn$ also increases the temperature jump, which reduces the energy exchange, increases the mean temperature difference, and tends to decrease both Nu_T and Nu_{H2}. While the wall heat flux is independent of AR and $\beta_v Kn$ for the $H2$ boundary condition, the average wall heat flux for the constant wall temperature boundary condition is reduced for both decreasing AR, and increasing $\beta_v Kn$. These effects result in a less significant increase in Nu_T due to slip, when $\beta = 0$, and a more significant decrease in Nu_T with $\beta_v Kn$, when $\beta \neq 0$, compared to Nu_{H2}.

The results in Fig. 4 also indicate that second-order temperature jump terms become more significant as $\beta_v Kn$ increases. For the constant wall temperature boundary condition the average wall normal first-order temperature gradient and the average wall normal second-order temperature gradient are of the opposite sign for all AR, β, and $\beta_v Kn$ evaluated. This causes the second-order Deissler boundary conditions to predict an increase in the temperature jump (decrease in Nu_T), compared to the first-order boundary condition data; while the second-order Karniadakis and Beskok boundary conditions predict a decrease in the temperature jump (increase in Nu_T), compared to the first-order boundary condition data. For the constant wall heat flux boundary condition, the average wall normal first-order temperature gradient and the average wall normal second-order temperature gradient are of the same sign for lower AR and $\beta_v Kn$ values, and of the opposite sign for increasing AR and $\beta_v Kn$ values. This causes the second-order Deissler boundary conditions to predict a decrease in temperature jump (increase in Nu_{H2}) for lower AR and $\beta_v Kn$, and an increase in temperature jump (decrease in Nu_{H2}) for higher AR and $\beta_v Kn$, compared to first-order boundary condition data; while the second-order Karniadakis and Beskok boundary conditions predict an increase in temperature jump (decrease in Nu_{H2}) for lower AR and $\beta_v Kn$, and a decrease in temperature jump (increase in Nu_{H2}) at higher AR and $\beta_v Kn$, compared to first-order boundary condition data.

5

Copyright © 2007 by ASME

Creep Flow Effects

The effect of creep flow on fully developed Po/Po_o and Nu/Nu_o is presented in Figs. 5 and 6 respectively, for creep velocity to mean velocity ratios of -0.25, 0.00, and 0.25, and for AR = 1, 2, 5, and ∞. For these data first-order slip boundary conditions are used, Pe = 0.5, and viscous dissipation effects are neglected. Nu_T data are not presented, as creep flow is negligible for thermally fully developed constant wall temperature boundary conditions. Also, because creep flow is zero at $\beta_v Kn$ = 0.00, creep flow effects on Po/Po_o and Nu/Nu_o are not presented for $\beta_v Kn$ less than 0.01. Positive u_c/u_m, creep flow in the same direction as the mean flow, is the result of heating; while negative u_c/u_m, creep flow in the opposite direction of the mean flow, is the result of cooling.

The data in Fig. 5 demonstrate that in addition to the AR and $\beta_v Kn$ effects previously discussed, positive u_c/u_m decreases Po/Po_o for all AR, while negative u_c/u_m increases Po/Po_o for all AR. Positive u_c/u_m increases the total slip velocity, which decreases the average wall shear stress and reduces Po/Po_o. Conversely, negative u_c/u_m decreases the total slip velocity at the wall which increases the average wall shear stress, thereby increasing Po/Po_o. Also, because positive u_c/u_m reduces the average wall shear stress there is less of a decrease in Po/Po_o with $\beta_v Kn$, and because negative u_c/u_m increases the average wall shear stress there is more of a decrease in Po/Po_o with $\beta_v Kn$.

There are several factors that contribute to the creep flow effect on Nu_{H2}, as presented in Fig. 6. Creep flow in the same direction as the mean flow increases the total slip velocity, which increases the energy exchange near the wall and tends to increase Nu_{H2}. Creep flow in the opposite direction of the mean flow decreases the total slip velocity, which decreases the energy exchange near the wall and tends to decrease Nu_{H2}. However, as rarefaction increases, the effect of the increasing temperature jump at the wall, for $\beta \neq 0$, and decreasing velocity gradients decrease the energy exchange, which increases the mean temperature difference and reduces Nu_{H2}, as well as the effect of u_c/u_m on Nu_{H2}. Although Nu_{H2} for AR = ∞ follows the same general trends as Nu_{H2} for AR = 1, 2, and 5 the effects of creep flow are reduced without the heat flux and creep flow contribution from the two side walls.
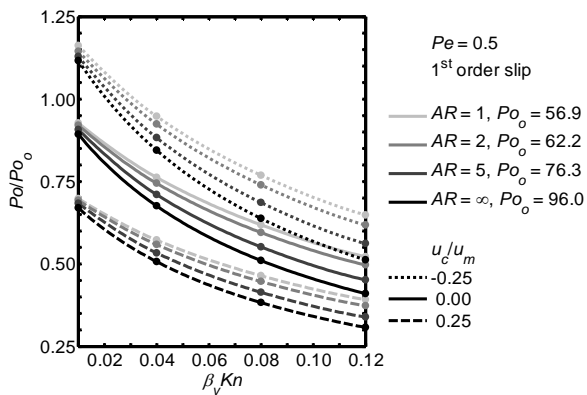
a)

AR = 1, Nu_o = 3.09
Pe = 0.5
Br_{H2} = 0
1st order slip

u_c/u_m
- - - 0.25
——— 0.00
········ -0.25

b)

AR = 2, Nu_o = 3.02
Pe = 0.5
Br_{H2} = 0
1st order slip

u_c/u_m
- - - 0.25
——— 0.00
········ -0.25

c)

AR = 5, Nu_o = 2.93
Pe = 0.5
Br_{H2} = 0
1st order slip

u_c/u_m
- - - 0.25
——— 0.00
········ -0.25

d)

AR = ∞, Nu_o = 8.23
Pe = 0.5
Br_{H2} = 0
1st order slip

u_c/u_m
- - - 0.25
——— 0.00
········ -0.25

Figure 6. Effect of creep flow on fully developed Nu_{H2}/Nu_o.
a) AR = 1, b) AR = 2, c) AR = 5, d) AR = ∞

Pe = 0.5
1st order slip

——— AR = 1, Po_o = 56.9
——— AR = 2, Po_o = 62.2
——— AR = 5, Po_o = 76.3
——— AR = ∞, Po_o = 96.0

u_c/u_m
········ -0.25
——— 0.00
- - - 0.25

Figure 5. Effect of creep flow on fully developed Po/Po_o.

a)

b)

c)

d)

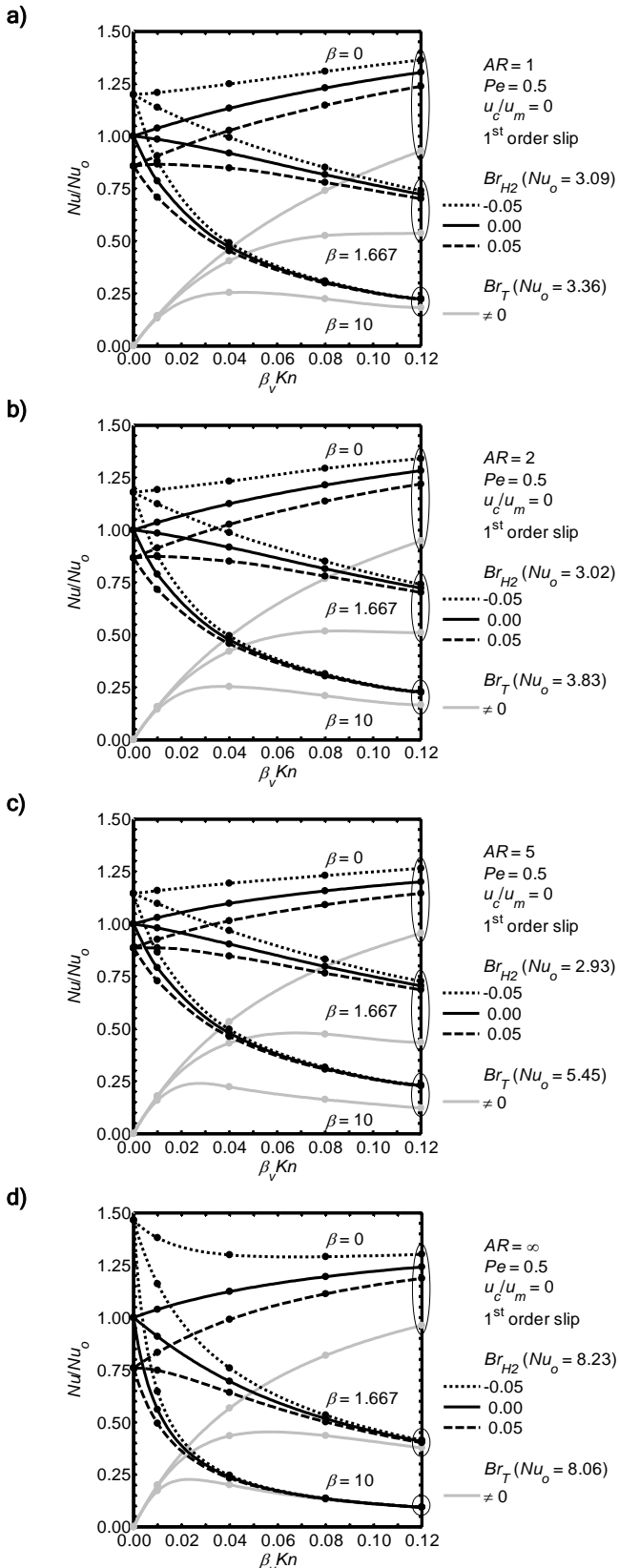**Figure 7. Effect of viscous dissipation and flow work on fully developed Nu_{H2}/Nu_o and Nu_T/Nu_o. a) $AR = 1$, b) $AR = 2$, c) $AR = 5$, d) $AR = \infty$**

Viscous Dissipation Effects

The effects of viscous dissipation and pressure work on fully developed Nu_{H2} and Nu_T and are given in Fig. 7 for $AR = 1$, 2, 5, and ∞. For these data, first-order slip boundary conditions are used, $Pe = 0.5$, and $u_c/u_m = 0$. Because μ is assumed to be constant, viscous dissipation has no additional effect on Po/Po_o. The Po/Po_o data corresponding to the data in Fig. 7 are the same as that given in Fig. 4 for first-order slip boundary conditions.

The Nu_{H2} data in Fig. 7 demonstrate that in addition to the AR and $\beta_v Kn$ effects previously discussed, positive Br_{H2}, heating, decreases Nu/Nu_o for all AR, while negative Br_{H2}, cooling, increases Nu/Nu_o for all AR. Note that Nu/Nu_o is unaffected by the pressure work contribution [13]. For heating, viscous dissipation increases the difference between the mixed mean temperature and the average wall temperature, thereby reducing Nu/Nu_o. For cooling, viscous dissipation decreases the difference between the mixed mean temperature and the average wall temperature, thereby increasing Nu/Nu_o. The effects of viscous dissipation are reduced for increasing rarefaction. This is due to the reduced velocity gradients caused by increasing slip. Although, Nu_{H2} for $AR = \infty$ follows the same general trends as Nu_{H2} for $AR = 1$, 2, and 5, the effects of viscous dissipation are increased without the heat flux contribution from the two side walls.

The Nu_T data presented in Fig. 7 were obtained for $Pe = 0.5$ and $Br_T = -0.2$ however, for a given $\beta_v Kn$, β, AR, and slip boundary condition model, all incompressible flows with both viscous dissipation and flow work result in the same fully developed value of Nu_T, regardless of the value of Pe or Br_T. For continuum flow, $\beta_v Kn = 0$, the effect of viscous dissipation, which generates thermal energy primarily near the wall, due to the larger velocity gradients, is balanced by the effect of flow work, which absorbs thermal energy, predominantly near the center of the flow due to the larger velocity magnitudes [13]. The result is a net wall heat flux of zero, and therefore $Nu_T = 0$. Within the slip flow regime, the slip velocity results in thermal energy generation, due to shear work, at the boundaries. This creates a nonzero wall heat flux and therefore a nonzero Nu_T. The shear work at the wall is dependent on both the slip velocity and the average wall shear stress. As $\beta_v Kn$ increases, the slip velocity increases, and for the lower slip flow regime this increases the shear work and therefore increases Nu_T. However, as the slip velocity increases the average wall velocity gradients throughout the flow are also reduced. This reduces viscous dissipation within the fluid, increases the flow work near the wall and for the upper end of the slip regime leads to a decrease in the shear work at the wall. These effects, combined with the effect of the temperature jump, β, and AR result in the Nu_T trends displayed in Fig. 7 [12].

SUMMARY AND CONCLUSIONS

The Poiseuille and Nusselt numbers for rectangular microchannels with both constant wall heat flux and constant wall temperature boundary conditions in the slip regime have been numerically calculated and compared. The resulting Po, Nu_{H2}, and Nu_T include the effects of second-order velocity slip and temperature jump boundary conditions, creep flow, and viscous dissipation with flow work. The numerical results for Po, Nu_{H2}, and Nu_T are presented in terms of the degree of rarefaction ($\beta_v Kn$); the gas/wall interaction parameter (β); creep

7 Copyright © 2007 by ASME

flow (u_c/u_m); and viscous dissipation (Br_{H2} or Br_T). These results are valid for incompressible or nearly incompressible, locally fully developed, steady state flows. The numerical solutions for microchannel Po, Nu_{H2}, and Nu_T have been calculated using a continuum based three-dimensional, unsteady, compressible, CFD algorithm modified with slip boundary conditions.

The results of this study indicate that the effects of second-order slip boundary conditions, creep flow, and viscous dissipation with flow work are all significant within the slip flow regime for rectangular microchannels pressure losses and convective heat transfer rates. The significance of each of these terms depends on the degree of rarefaction, the gas/wall interactions, and the thermal boundary condition. The effects of second-order boundary conditions increase as rarefaction increases, with the two models studied having opposite effects when compared to first-order boundary conditions. The accuracy of solutions generated with the second-order boundary conditions requires comparison with experimental data, which does not currently exist. Creep flow results in an increase in Nu_{H2} for heating and decrease in Nu_{H2} for cooling by an amount dependant on u_c/u_m, $\beta_v Kn$, β, and AR. Viscous dissipation increases Nu_{H2} for cooling and decreases Nu_{H2} for heating as a function of Br_{H2}, $\beta_v Kn$, β, and AR. The combined effects of viscous dissipation, flow work, and shear work within the slip flow regime cause Nu_T to increase with increasing $\beta_v Kn$, by an amount dependent on AR and β.

REFERENCES

[1] Maxwell, J.C., 1879, "On stresses in rarified gases arising from inequalities of temperature," Philosophical Transactions of the Royal Society of. London, 170, pp. 231-256.

[2] Smoluchowski, M., 1898, "Ueber wärmeleitung in verdünnten gasen," Annalen der Physik und Chemie, 64, pp. 101-130.

[3] Deissler, R.G., 1964, "An analysis of second-order slip flow and temperature-jump boundary conditions for rarefied gases," International Journal of Heat and Mass Transfer, 7, pp. 681-694.

[4] Karniadakis, G.E. and Beskok, A., 2002, "Micro Flows: Fundamentals and Simulation," Springer-Verlag, New York.

[5] Maurer, J., Tabeling, P., Joseph, P., Willaime, H., 2003, "Second-order slip laws in microchannels for Helium and Nitrogen," Physics of Fluids, 15(9), pp. 2613-2621.

[6] Colin, S., Lalonde, P., Caen, R., 2004, "Validation of a second-order slip flow model in rectangular microchannels," Heat Transfer Engineering, 25(3), pp. 23-30.

[7] Ji, Y., Yuan, K., Chung, J.N., 2006, "Numerical simulation of wall roughness on gaseous flow and heat transfer in a microchannel," International Journal of Heat and Mass Transfer, 49, pp. 1329-1339.

[8] Xiao, N., Elsnab, J., Ameel, T., 2006, "Microtube gas flows with second-order slip flow and temperature jump boundary conditions," Proceeding of Fourth International Conference on Nanochannels, Microchannels and Minichannels.

[9] Zhu, X., Liao, Q., Xin, M.D., 2006, "Gas flow in microchannel of arbitrary shape in slip flow regime," Nanoscale and Microscale Thermophysical Engineering, 10, pp. 41-54.

[10] van Rij, J., Harman, T., Ameel, T., 2007, "The effect of creep flow on two-dimensional isoflux microchannels," International Journal of Thermal Sciences, article in press.

[11] van Rij, J., Ameel, T., Harman, T., 2006, "The effect of viscous dissipation on two-dimensional microchannel heat transfer," Proceedings of ASME International Engineering Congress and Exposition.

[12] van Rij, J., Ameel, T., Harman, T., 2007, "Constant wall temperature Nusselt and Poiseuille numbers in rectangular microchannels," Proceedings of ASME-JSME Thermal Engineering Summer Heat Transfer Conference.

[13] Ou, J.W., Cheng, K.C., 1973, "Effects of pressure work and viscous dissipation on Graetz problem for gas flows in parallel-plate channels," Wärme- und Stoffübertragung., 6, pp. 191-198.

[14] Tunc, G., Bayazitoglu, Y., 2001, "Heat transfer in microtubes with viscous dissipation," International Journal of Heat and Mass Transfer, 44, pp. 2395-2403.

[15] Hadjiconstantinou, N.G., "Dissipation in small scale gaseous flows," Journal of Heat Transfer, 125, pp. 944-947.

[16] Aynur, T.N., Kuddusi, L., Eğrican, N., 2006, "Viscous dissipation effect on heat transfer characteristics of rectangular microchannels under slip flow regime and H1 boundary conditions," International Journal of Heat and Mass Transfer, 42, pp. 1093-1101.

[17] Jeong, H., Jeong, J, 2006, "Extended Graetz problem including streamwise conduction and viscous dissipation in microchannel," International Journal of Heat and Mass Transfer, 49, pp. 2151-2157.

[18] Aydin, O., Avci, M., 2006, "Thermally developing flow in microchannels," Journal of Thermophysics, 20(3), pp. 628-632.

[19] Chen, C., 2006, "Slip-flow heat transfer in a microchannel with viscous dissipation," International Journal of Heat and Mass Transfer, 42, pp. 853-860.

[20] Harlow, F., Amsden, A., 1968, "Numerical calculation of almost incompressible flow," Journal of Computational Physics, 3, pp. 80-93.

[21] Kashiwa, B., Rauenzahn, R., 1994, "A cell-centered ICE method for multiphase flow simulations," Los Alamos National Laboratory Technical Report, LA-UR-93-3922.

[22] Parker, S.G., Guilkey, J., Harman, T., 2006, "A component-based parallel infrastructure for the simulation of fluid-structure interaction," Engineering with Computers, 22, pp. 277-292.

[23] Tunc, G., Bayazitoglu, Y., 2002, "Heat transfer in rectangular microchannels," International Journal of Heat and Mass Transfer, 45, 765-773.

[24] Yu, S., 2002, "Slip flow heat transfer in rectangular microchannels," Ph.D. Dissertation, University of Utah.

[25] Shah, R.K., London, A.L., 1978, "Laminar Flow Forced Convection in Ducts," Academic Press, New York.

[26] Spiga, M., Morini, G.L., 1996, "Nusselt numbers in laminar flow for H2 boundary conditions," International Journal of Heat and Mass Transfer, 39(6), pp. 1165-1174.